Atomic nitrogen production in nanosecond tube discharges

Inna Orel, Tat Loon Chng, N.A. Popov, Svetlana Starikovskaia

▶ **To cite this version:**

Inna Orel, Tat Loon Chng, N.A. Popov, Svetlana Starikovskaia. Atomic nitrogen production in nanosecond tube discharges. 24th International Symposium on Plasma Chemistry (ISPC 24), Jun 2019, Naples, Italy. hal-02407647

HAL Id: hal-02407647
https://hal.science/hal-02407647

Submitted on 6 Jan 2021

HAL is a multi-disciplinary open access archive for the deposit and dissemination of scientific research documents, whether they are published or not. The documents may come from teaching and research institutions in France or abroad, or from public or private research centers.

L'archive ouverte pluridisciplinaire **HAL**, est destinée au dépôt et à la diffusion de documents scientifiques de niveau recherche, publiés ou non, émanant des établissements d'enseignement et de recherche français ou étrangers, des laboratoires publics ou privés.

Atomic nitrogen production in nanosecond tube discharges

I. S. Orel[1*], T. L Chng[1], N. A. Popov[2] and S. M. Starikovskaia[1]

[1]*Laboratory of Plasma Physics (CNRS, Ecole Polytechnique, Sorbonne University, University Paris-Sud, Observatoire de Paris, University Paris-Saclay) Palaiseau, 91128, France*
[2]*Skobeltsyn Institute of Nuclear Physics, Moscow State University, Moscow, 119991, Leninsky gory, Russia*

Abstract: Two photon absorption laser-induced fluorescence is used to make measurements of atomic nitrogen density in nanosecond tube discharges under different conditions of specific energy deposition. The data reveals that the atomic nitrogen dissociation fraction is a strong function of this energy loading (measured in electronvolts per molecule or eV/mol), ranging from a few tenths to hundredths of a percent for 10^{-3} eV/mol to more than 10% for around 2 eV/mol.

Keywords: TALIF, nanosecond discharge, nitrogen, fast ionization wave.

1. Introduction

This work is motivated by a fundamental interest in the atomic nitrogen (N) production associated with nanosecond discharges as a function of the reduced electric field. Good predictive knowledge of this behaviour and the associated chemical pathways, particularly at higher reduced fields (> several hundred Td) synonymous with nanosecond discharges, is essential for improved plasma kinetic models and could lead to the development of more efficient sources of N atom production. More fundamentally, due to its low loss rate through slow atom-atom recombination, N atoms are an important energy storage channel for non-equilibrium molecular nitrogen (N_2) plasmas. Over the past half a decade or so, several numerical studies have attempted to characterize the N atom production or energy cost as a function of the reduced electric field [1,2]. These studies have found that the energetic cost of N atom production drops drastically with increasing reduced field. However, existing experimental data which describes this functional dependence is relatively scattered and it is timely that a systematic experimental study be carried out. Here, we choose to vary the reduced electric field by changing the geometric dimensions of the discharge tube which in turn serves as a convenient way of modifying the corresponding specific energy coupled to the plasma.

2. Experimental setup

The discharge setup employed in this study is typical of a fast ionization wave (FIW) discharge [3]. FIW discharges commonly comprise of a cylindrical tube of length L and diameter d (where $L >> d$), which is sandwiched between two electrodes. The discharge is initiated by applying high voltage (HV) pulses of nanosecond duration at gas pressures ranging from 1-100 Torr. While the physics of FIW development are beyond the scope of this study, it should be pointed out that the use of such a discharge setup is favoured for its superior spatial homogeneity relative to its counterparts such as streamer discharges. FIW discharges are therefore a common choice of platform for experimental species measurements.

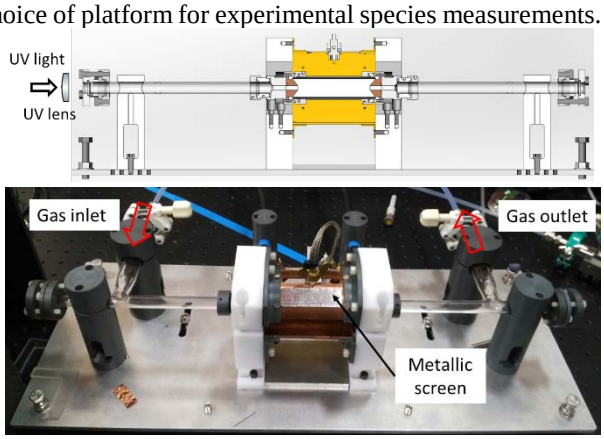

Fig. 1. a) Cross-sectional view of discharge setup. Brass electrodes and the metallic screen are coloured in brown and yellow respectively. The laser light for the two-photon excitation is focused along the tube axis from left to right. b) Picture of discharge setup. (Electrodes and discharge tube are concealed.)

Two different FIW discharge setups are utilized in this study. A schematic of the main discharge cell geometry is presented in Fig. 1. A cylindrical quartz tube with a nominal length of 90 mm and an internal and external diameter of 20 mm and 24 mm respectively, sits between two hollow semi-conical brass electrodes with an inter-electrode gap distance of 80 mm. The discharge cell is partially encapsulated by a cylindrical metallic screen in an annular fashion. Pure N_2 gas at a pressure of 20 mbar enters and exits the capillary via two glass side arms – respectively located just upstream and downstream of the discharge tube – at a flow rate of 10 sccm. This flow rate and pressure was chosen based on the results of a separate optical emission study, which highlighted the presence of spatial inhomogeneities near the tube wall, particularly in pure N_2 (versus air) as well as at higher flow rates and working pressures. At the same time, this preference for a

lower pressure and flow rate had to be balanced against opposing considerations for optimizing energy deposition (see Fig. 2) and ensuring adequate gas renewal before each successive high voltage pulse. For the present flow rate of 10 sccm and 10 Hz pulse repetition rate (see two paragraphs below for the specifics of the applied voltage), gas renewal was calculated to take place after a sequence of 17 pulses.

The other discharge cell used is similar in concept to the foregoing setup, except with a significantly smaller diameter. Instead, a quartz capillary with an internal diameter of 1.7 mm and inter-electrode gap distance of 67 mm is used. This configuration has been described in detail in [4] and is very similar to that previously used in [5]. As illustrated in Fig. 2, modification of the tube diameter is an effective and convenient means of altering the specific energy delivered to the plasma, as well as the attendant reduced electric field. While these measurements were performed in air, it is expected that these trends should be relatively well preserved for the case of pure N_2.

High voltage nanosecond pulses are delivered by means of a FPG 12-1NM high-voltage generator (HVG) manufactured by FID GmbH. Positive polarity, 9.3 kV amplitude voltage waveforms with a rise time of 4 ns and a full width at half maximum (FWHM) of 30 ns are produced by this high voltage source at a repetition rate of 10 Hz. A RG213 coaxial cable connects the HVG to the discharge cell and a second such cable of identical length is attached to the remaining electrode but kept ungrounded at a floating potential. The shielding of both these coaxial cables is connected to the metallic screen. Due to an impedance mismatch between the high voltage pulses and the discharge, a series of pulse reflections occur and leads to a sequence of 3 incident pulses with gradually diminishing voltage seen by the discharge, each separated by about 250 ns. Custom-made, calibrated back current shunts are installed at mid-length of both coaxial cables for measuring the specific energy coupled to the plasma.

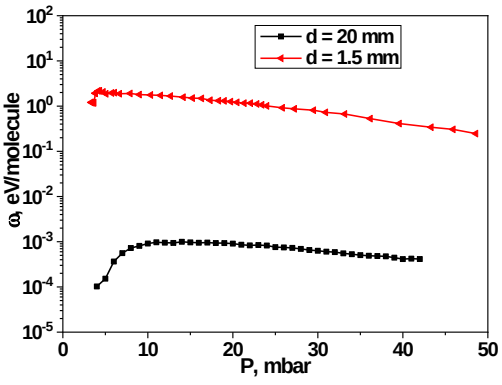

Fig. 2. Specific energy deposition, ω as a function of pressure (in air) for tubes of different diameters: red curve taken from [6] is for the capillary tube; d=1.7 mm, black curve is for a larger diameter, d=20 mm tube.

The laser system used for the TALIF experiments consists of a Sirah Lasertechnik Cobra Stretch dual-grating dye laser, which produces output within the desired range of 621 nm at a repetition rate of 10 Hz. This light is then frequency-tripled via two successive alpha-BBO non-linear crystals so as to yield 3 mJ, tunable UV pulses near 207 nm (at the same repetition rate) with a pulse duration of about 6.5 ns.

The N TALIF scheme used for these experiments is shown in Fig. 3a). The two-photon 3p $^4S_{3/2}$ N resonance is accessed via a pair of 206.7 nm photons and subsequently fluoresces to three different fine structure levels, emitting light respectively at 742.6 nm, 744.4 nm and 747.0 nm [7]. This resulting fluorescence is captured by an infra-red (IR) sensitive Hamamatsu photomultiplier with an attached bandpass filter (centre wavelength 750 nm, 10 nm FWHM). Signals are obtained by averaging over 400 laser shots within a laser intensity fluctuation of ±3%.

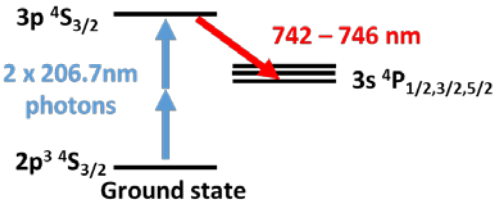

a)

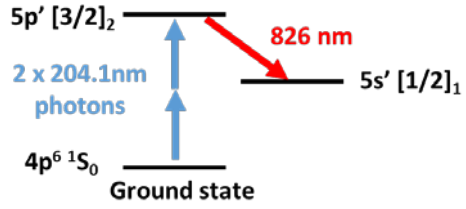

b)

Fig. 3. a) N atom and b) Kr atom TALIF scheme.

In order to obtain quantitative N densities, signal calibration against an inert, reference gas – in this case krypton – was performed in a manner similar to that in [8]. The corresponding Kr TALIF scheme involves pumping the 5p'[3/2]$_2$ resonance with two photons at 204.1 nm, followed by fluorescence to the 5s'[1/2]$_1$ state at 826 nm (see Fig. 3b)). For these Kr experiments, a 10 nm narrow bandpass filter centred at 830 nm is used to spectrally isolate the atomic fluorescence. Based on the derivation provided in [8], the number density of atomic nitrogen may be written as:

$$n_N = \left(\frac{\sigma_{Kr}}{\sigma_N}\right)\left(\frac{\nu_N}{\nu_{Kr}}\right)^2\left(\frac{PMT_{Kr}}{PMT_N}\right)\left(\frac{A_{Kr}}{A_N}\right)\left(\frac{F_{Kr}}{F_N}\right)\left(\frac{A_N+Q_N}{A_{Kr}+Q_{Kr}}\right)\left(\frac{I_{Kr}}{I_N}\right)^2\left(\frac{S_N}{S_{Kr}}\right)n_{Kr} \qquad (1)$$

where n is the number density, σ is the two-photon absorption cross-section, ν is the resonance frequency, PMT is the photomultiplier sensitivity at the resonant wavelength(s), A is the natural radiative rate, F is the filter transmission, Q is the quenching rate of the two-photon excited state, I is the laser intensity and S is the spectrally and temporally integrated fluorescence measured by the

photomultiplier. Subscripts N and Kr refer to atomic nitrogen and krypton respectively. The ratio of two-photon cross-sections (value of 0.67) is obtained from [8]; PMT sensitivities and filter transmission curves are obtained or extrapolated from their respective manuals. The natural radiative rate of N (value of 29.6 ns) is obtained from [8], while the Kr number density of 6.7 x 10^{16} cm^{-3} is attained by flowing Kr gas at room temperature through the capillary at a pressure of 2.7 mbar.

To ensure that the fluorescence signal *S* observes a quadratic dependence on the laser intensity (see eqn. (1)), the laser energy was varied over a range of 10-300 µJ in order to establish the optimum laser intensity. The energy used for the N and Kr experiments were 200 µJ and 30 µJ respectively for the large tube and 85 µJ and 30 µJ for the capillary. As will be seen later, the higher energy requirements for the large tube (versus the capillary) were a consequence of the comparatively lower N densities (i.e. weaker signals).

An important distinction should be made with regards to the two-photon pumping for the two different discharge setups. For the discharge setup in Fig. 1, the UV light is focused with a 50 cm focal length lens along an axis parallel to the length of the tube. Assuming a Gaussian beam, this leads to an effective probe length or confocal beam parameter of about 1.5 cm. The resulting fluorescence is collected along an axis orthogonal to the pump beam propagation. On the contrary, due to the small diameter of the quartz capillary, the UV excitation (using the same lens) is directed along an axis perpendicular to the length of the capillary, and the fluorescence collected at 90° from this axis [4]. For this latter case, the fluorescence signal is estimated to originate from the entire 1.7 mm diameter of the capillary.

3. Results and discussion

Shown in Fig. 4 are the N atom density time evolution curves for the two different discharge tubes. These measurements are obtained by integrating the resonant fluorescence signals captured by the photomultiplier (PMT) for both Kr and N, and substituting the relevant values into equation (1). To minimize the possibility of laser photolytic interferences from within the discharge as well as in the surrounding air, it was verified that no measurable signals were present when the discharge was turned off. The data in Fig. 4a have been corrected for excited quenching; quenching rates are determined by fitting an exponential function to the decaying section of the PMT signals. Unfortunately, due to limited signal sensitivity associated with background plasma emission and electromagnetic interference, data was only faithfully recorded beginning from 5 µs after the discharge initiation. Fig. 4b shows a similar such plot for the capillary discharge, except for the fact that some of the signals measured in the early afterglow till around 10 µs are plagued by strong quenching and are left uncorrected. The origin of this quenching behaviour is unclear but could be related to the unique plasma chemistry associated with the high levels of specific delivered energy for the capillary discharge. This would augment the production of electrons, N atoms and other excited state species, all of which are effective excited state 'quenchers'. In addition, the unusually large production of excited state species could also lead to fast gas heating (viz. temperature rise) [5] that also acts to increase the quenching rate.

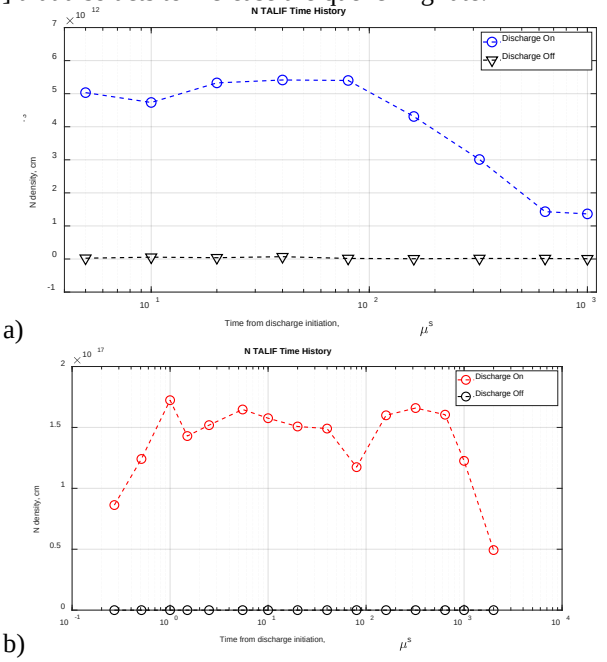

a)

b)

Fig. 4. Temporal evolution of N atom density in a) 20 mm diameter tube and b) 1.7 mm diameter capillary.

Unlike the larger 20 mm tube, in the case of the capillary it was possible to acquire good signals after each high voltage pulse; in fact, the first data point corresponds to a time instant of about 270 ns after the start of the discharge. Under these conditions, the data in Fig. 4b indicates that each subsequent high voltage pulse continues to add a considerable amount of N atoms to the system. Since the specific delivered energy in the second and third pulses are substantially lower than the first, it is possible that the rise in the ground state N atom density in these instances could be attributable to the quenching of excited N(^{2}D) atoms. The efficiency of this process increases with temperature as reported in [9]. This hypothesis is further supported by previous measurements in a capillary discharge which confirm a consistent rise in the gas temperature (after the second and third pulses) due to fast gas heating mechanisms [5].

A principal result of Fig. 4 is that the significant disparity in the levels of specific delivered energy for both discharges yields a correspondingly large difference in the N atom production. More specifically, for the same order of gas pressure, the N atom production in the capillary is about 4-5 orders of magnitude higher. It is impressive that the peak dissociation fraction attained for the capillary discharge is slightly more than 11%.

Here, the dissociation fraction γ is defined as:

$$\gamma = \left(\frac{n_N}{2n_{N_2}}\right) \qquad (2)$$

While this outcome is by no means unexpected, it should be pointed out that such high levels of dissociation (> 10%) are extremely difficult to achieve using DC discharges and has only been reported in the literature in rare instances such as [10]. This holds promise for developing the capillary discharge as an efficient source of N atom production.

In contrast to the distinct levels of N atom production in both discharges, what is consistent is the long-lived nature of these atomic species. Due to the slow atom-atom recombination and wall recombination rates as calculated in [4], it is thus unsurprising that non-negligible N atom densities are still detected even 1 ms after the start of the discharge. It must therefore be emphasized that modelling efforts which attempt to predict the kinetics for pulsed discharges with repetition rates that exceed the relevant recombination times should necessarily take into account these residual species.

4. Conclusions and future work

The present study has examined the N atom densities produced in two separate discharge cells with vastly differing levels of specific delivered energy. The results show that the N atom densities exhibit a strong correlation with the specific delivered energy to the plasma. Ongoing research is continuing on two fronts: (i) further N atom TALIF measurements at other different levels of specific delivered energy and (ii) comparing these results and the energy cost per atom with a high fidelity kinetic model.

5. Acknowledgements

This work was partially supported by the French National Research Agency, ANR (ASPEN Project), LabEx Plas@Par and the French–Russian international laboratory LIA KaPPA 'Kinetics and Physics of Pulsed Plasmas and their Afterglow (including RFBR project 17-52-16001 and CNRS financial and organization support)'.

6. References

[1] N. Popov, Plasma Physics Reports, **39(5),** 420 (2013)
[2] D. Tsyganov, & S. Pancheshnyi, Plasma Sources Science and Technology, **21(6)**, 065010 (2012).
[3] L. Vasilyak, S. Kostyuchenko, N. Kudryavtsev, & I. Filyugin, Physics-Uspekhi, **37(3)**, 247 (1994).
[4] T. Chng, N. Lepikhin, I. Orel, N. Popov, & S. Starikovskaia, AIAA Scitech Meeting, (2019) *submitted.*
[5] N. Lepikhin, N. Popov, & S. Starikovskaia, Plasma Sources Science and Technology, **27(5)**, 055005 (2018).
[6] A. Klochko, PhD thesis, Ecole Polytechnique, Palaiseau, France, (2014)
[7] A. Kramida, Y. Ralchenko, J. Reader, & NIST ASD Team, NIST Atomic Spectra Database (version 5.5.6), 2018.
[8] K. Niemi, V. Schulz-Von Der Gathen, & H. Döbele, Journal of Physics D: Applied Physics, **34(15)**, 2330 (2001).
[9] B. Galvão, A. Varandas, J. Braga, & J. Belchior, The Journal of Physical Chemistry Letters, **4(14)**, 2292 (2013)
[10] T. Czerwiec, F. Greer, & D. Graves, Journal of Physics D: Applied Physics, **38(24)**, 4278 (2005).